Ligand Pose Predictions for Human G Protein-Coupled Receptors: Insights from the Amber-based Hybrid Molecular Mechanics/Coarse-Grained Approach

Jakob Schneider,[*,†,‡,¶] Ksenia Korshunova,[†,‡] Zeineb Si Chaib,[†,§] Alejandro Giorgetti,[†,‖,⊥] Mercedes Alfonso-Prieto,[†,#,⊥] and Paolo Carloni[†,‡,¶,⊥]

†*Computational Biomedicine, Institute for Advanced Simulations IAS-5/Institute for Neuroscience and Medicine INM-9, Forschungszentrum Jülich GmbH, 52428 Jülich, Germany.*

‡*Department of Physics, RWTH Aachen University, 52074 Aachen, Germany.*

¶*JARA-Institute: Molecular Neuroscience and Neuroimaging, Institute for Neuroscience and Medicine INM-11/JARA-BRAIN Institute JBI-2, Forschungszentrum Jülich GmbH, 52428 Jülich, Germany.*

§*RWTH Aachen University, 52062 Aachen, Germany.*

‖*Department of Biotechnology, University of Verona, 37314 Verona, Italy.*

⊥*JARA–HPC, IAS-5/INM-9 Computational Biomedicine, Forschungszentrum Jülich GmbH, 52428 Jülich, Germany.*

#*Cécile and Oskar Vogt Institute for Brain Research, Medical Faculty, Heinrich Heine University Düsseldorf, 40225 Düsseldorf, Germany.*

E-mail: ja.schneider@fz-juelich.de

Abstract

Human G protein-coupled receptors (hGPCRs) are the most frequent targets of FDA-approved drugs. Structural bioinformatics, along with molecular simulation, can support structure-based drug design targeting hGPCRs. In this context, several years ago, we developed a hybrid Molecular Mechanics (MM)/Coarse-Grained (CG) approach to predict ligand poses in low resolution hGPCR models. The approach was based on the GROMOS96 43A1 and PRODRG united-atom force fields for the MM part. Here, we present a new MM/CG implementation using instead the Amber 14SB and GAFF all-atom potentials for proteins and ligands, respectively. The new implementation outperforms the previous one, as shown by a variety of applications on models of hGPCR/ligand complexes at different resolution, and it is also more user-friendly. Thus, it emerges as a useful tool to predict poses in low resolution models and provides insights into ligand binding similarly to all-atom molecular dynamics, albeit at a lower computational cost.

Introduction

Human G protein-coupled receptors (hGPCRs) are the largest family of transmembrane proteins (4 % in the human genome[1]), with ≈800 members. These receptors, which serve as signal transmitters across the cell membrane, are very important from a pharmaceutical perspective. About one third of FDA approved drugs target ≈100 hGPCRs[2]; many others (including about 400 human odorant and 25 human bitter taste receptors), are highly promising drug targets[3–5].

While chemoinformatics approaches are highly useful to identify drug leads across the entire superfamily[6], rational drug development is limited by the lack of experimental structural information. For most hGPCRs (92 %)[7], one has to resort to computational models. Unfortunately, bioinformatics-based predictions have limitations due to the low sequence identity shared across the superfamily[8]. The predictions can, however, be improved by

using molecular simulation[9–15]. In this regard, our team has developed a hybrid Molecular Mechanics/Coarse-Grained (MM/CG) approach tailored to predict ligand poses in hGPCRs[16–18]. Here, the "MM" part consists of the ligand and the binding site, as well as surrounding water molecules. So far, this region has been described using the GROMOS96 43A1 united atom force field[19] for the protein, together with the PRODRG force field[20] for the ligand (hereafter, GROMOS-based MM/CG). The rest of the protein (CG region) has been described by a Gō model[21]. This allows for preserving the overall flexibility of the system[22,23], while reducing its overall complexity. Moreover, it minimizes possible structural issues introduced by non-optimal side chain orientations in low resolution homology models, i.e. built based on templates sharing sequence identity below 35 %[13,24–26]. The membrane has been represented implicitly, further reducing the size of the system. The GROMOS-based MM/CG scheme has been applied to a variety of hGPCRs, from the β2-adrenergic receptor (β2-AR) in complex with antagonists carazolol and isoprenaline[16,27], to bitter taste receptors (hTAS2R) bound to agonists[27–29] and GPR3 with a synthetic agonist[30]. The GROMOS-based MM/CG simulations for these complexes turned out to be consistent with the available experimental data. Simulations of the β2-AR/carazolol complex reproduced the crystallographic ligand pose, regardless of the resolution of the initial structure (either a high resolution X-ray structure[16] or a low resolution homology model[27]). In particular, the predicted receptor–ligand interactions were consistent with those in the X-ray structure[31] and in previous all-atom (AA) Amber(99SB)-based molecular dynamics (MD) simulations[32], though protein–ligand distance distributions were slightly different[16]. The initial structure of the β2-AR/isoprenaline complex was generated using an X-ray structure of the same receptor bound to carazolol. The subsequent GROMOS-based MM/CG simulation was in good agreement with previous AA-MD simulations[32]. In contrast, for the hTAS2R- and GPR3-ligand complexes[27–30], only low resolution models could be built and the only experimental data available for validation were mutagenesis experiments, which may pinpoint specific residues involved in ligand binding[13]. The GROMOS-based MM/CG simulations identified most of

the experimentally determined binding residues[27–30], improving remarkably the predictions of molecular docking[13,29].

Here, we present a new implementation of the MM/CG approach. It uses the Amber 14SB[33] and GAFF[34] all-atom force fields for the MM part of the receptor (hereafter, Amber-based MM/CG). Such implementation has two major advantages. First, a small molecule force field (GAFF[34]) has been specifically designed for molecules of pharmaceutical relevance and it is compatible with the Amber protein force field[33]. Second, the ligand parameterization with GAFF can be automatized using ACPYPE[35], replacing the use of the external PRODRG webserver[20]. Thus, the Amber-based MM/CG implementation facilitates the automatization of the ligand parameterization and thereby accelerates the simulation setup for pharmaceutically relevant hGPCRs.

Here, we performed Amber-based MM/CG simulations for a variety of hGPCR/ligand complexes, using starting structures at different resolution. These benchmark systems were used, on one hand, to validate our new implementation, by comparing our results with X-ray structural information and/or all-atom and GROMOS-based MM/CG simulations. On the other, the results were compared with docking poses for models across different resolution regimes[9,36,37]. Specifically, we focused on four hGPCR/ligand complexes, using structural information of decreasing resolution, see Table 1).

(i) The human adenosine 2A receptor in complex with its antagonist caffeine ($hA_{2A}R$/CFF). Here, X-ray structural information[38] and all-atom Amber(99SB-ILDN)-based MD simulations[39] are available for *a posteriori* validation. The starting structure for the Amber-based MM/CG simulations carried out in this work was based on a snapshot of the latter.

(ii) The human β2-adrenergic receptor in complex with the agonist adrenaline (β2-AR/ADR). In this case, the Amber-based MM/CG simulations were started from two different models at different resolution. The available X-ray structure[40] was used to validate retrospectively our results. The first model was constructed using the structure of the same receptor co-crystallized with another agonist, the high-affinity ligand BI167107[40], similar

to the procedure followed previously for the β2-AR/carazolol complex[16,27]. ADR was then docked into the binding cavity. The two β2-AR ligands share the phenol ring and the hydroxylamine tail (Figure S9[41]). Thus, the predictive power of docking procedures in this case is expected to be very high[9,36,37]. The second model was built using a template with 24 % sequence identity, the M2 muscarinic acetylcholine receptor (M2R) in its active state conformation[42]. Here, docking predictions are challenging because of the low overall sequence identity, but they can still be successful, depending on the level of conservation of the ligand binding residues[9,43]. In this case, nine out of 41 ligand-contacting residues[44] are conserved.

(iii) The dopamine D3 receptor in complex with the antagonist eticlopride (D3R/ETI). Here, we built two homology models. The first one used the dopamine D4 receptor[45] as template. The two dopamine receptor subtypes share 41 % sequence identity, right above the 35 % to 40 % threshold suggested for successful docking to hGPCR homology models[9,46]. The second model was based on the M2R in an inactive state[47], a template with 31 % sequence identity and thus right below the aforementioned 35 % to 40 % threshold. Therefore, the two D3R models are expected to be medium- and low-resolution, respectively.

(iv) The human bitter taste receptor 16 in complex with phenyl-β-D-glucopyranoside (hTAS2R16/PGP). Only low resolution models can be built in this case, because the sequence identity of hTAS2Rs with any other hGPCR with available experimental structure is $<$ 20 %[13]. Under these circumstances, the predictive power of docking is highly limited[13]. The results were compared with previously reported mutagenesis data[48] and GROMOS-based MM/CG simulations[29].

The Amber-based MM/CG simulations on systems (i) and (iv) improve the ligand pose predictions relative to the GROMOS-based ones. The retrospective validation on systems (ii) and (iii) further shows the potential of Amber-based MM/CG simulations to identify protein–ligand interactions. Finally, the Amber-based MM/CG performs better than docking alone to predict binding residues for low-resolution models. For high-resolution models, where docking is usually highly successful[9,36,37], our simulations provide new insights into

the flexibility of receptor–ligand interactions and hydration of the binding cavity, at a lower expense than all-atom MD. Hence, the new implementation, which is freely available, is expected to assist the prediction of ligands and to shed light on flexibility and hydration of the binding site across hGPCRs (as well as GPCRs from other species).

Table 1: Overview of the hGPCR/ligand complexes studied in this work.

hGPCR/ligand complex[a]	MM/CG type[b]	Initial structural model[c]	Comparison to[d]			
			X-ray	AA-MD	mut. data	docking
$hA_{2A}R$/CFF (HR)	GROMOS	AA-MD snapshot	3RFM	✓	✓	✗
	Amber	AA-MD snapshot	3RFM	✓	✓	✗
β2-AR/ADR (HR)	Amber	Model (4LDE) + docking	4LDO	✗	✓	✓
β2-AR/ADR (LR)	Amber	HM (4MQS, 24 %) + docking	4LDO	✗	✓	✓
D3R/ETI (MR)	Amber	HM (5WIU, 41 %) + docking	3PBL	✗	✓	✓
D3R/ETI (LR)	Amber	HM (3UON, 31 %) + docking	3PBL	✗	✓	✓
hTAS2R16/PGP (LR)	GROMOS	HM (4LDE, 13 %) + docking	✗	✗	✓	✓
	Amber	GROMOS-based MM/CG frame	✗	✗	✓	✓

[a] HR, MR and LR denote high, medium and low resolution models, respectively.
[b] MM/CG simulations were either based on the Amber 14SB force field[33] or GROMOS 43A1 force field[49] for the protein MM part. hTAS2R16/PGP GROMOS simulations are taken from reference 29.
[c] The "AA-MD snapshot" was taken from an Amber99SB-ILDN-based AA-MD simulation[39]. "Model" was based on the X-ray structure of the same β2-AR[40]; thus the sequence identity is 100 %. "HM" refers to homology models (with template and sequence identity indicated between parentheses), followed by ligand docking with HADDOCK[50]. For the hTAS2R16/PGP complex, the GROMOS MM/CG trajectory was taken from reference 29; a snapshot of this simulation was used to start the Amber-based MM/CG simulations reported in this work.
[d] The results of the simulations were validated against available X-ray structures (PDB code shown), mutagenesis data[1,48,51–55] and/or AA-MD simulations[39], as indicated. The MM/CG-derived ligand poses are compared with those generated by docking (from reference 29 for hTAS2R16/PGP).

Methods

The next subsections provide details on the protocol for each of the computational methods used to predict ligand binding poses, i.e. HADDOCK-[50,56] and Glide Induced Fit Docking[57], as well as GROMOS- and AMBER-based MM/CG simulations. The standard protocols for each of these methods were used. Only in the cases of $hA_{2A}R$ and hTAS2R16/PGP these protocols were adjusted to be able to compare our results with published ones (see references 39 and 29, respectively).

Starting structures

The starting structure of $hA_{2A}R$ in complex with caffeine (system (i)) was taken from an AA-MD trajectory based on the Amber force field[39] (Table 1), while that of hTAS2R16/PGP (iv) was taken from a GROMOS-based MM/CG simulation of this receptor–ligand complex[29]. Two initial structures at different resolution were generated for each of the β2-AR/ADR (ii) and D3R/ETI (iii) complexes. The sequences of β2-AR and D3R were retrieved from the corresponding UniProt entries, i.e. P07550 and P35462, respectively. The extracellular N-termini (1-34 aa for β2-AR and 1-32 aa for D3R) were not included in the modeling because of the lack of templates covering this region.

For β2-AR, a high-resolution model (HR) was built based on the X-ray structure of the same receptor bound to a different ligand, i.e. the high-affinity agonist BI167107, and an engineered nanobody (PDB code 4LDE[40]), by reverting the thermostabilizing mutations and adding the missing intracellular loops. Thus, the model has effectively 100 % sequence identity. A second model was generated by homology modeling using as template the M2 muscarinic acetylcholine receptor in an active state bound to the agonist iperoxo (PDB code 4MQS[42]). The sequence identity is only 24 %, resulting in a low-resolution model (LR)[25,26].

For D3R, two inactive state models (as expected for D3R bound to the antagonist eticlopride) were generated using homology modeling (Table 1): (i) a medium resolution (MR)

model using as template the D4 dopamine receptor in complex with the antagonist nemonapride (PDB code 5WIU[45], sequence identity 41 %) and (ii) a LR model using as template the M2 muscarinic acetylcholine receptor bound to the antagonist 3-quinuclidinyl-benzilate (PDB code 3UON[47], sequence identity 31 %). Target-template sequence alignments were performed using the HHsearch[58] implementation within the GOMoDo webserver[59], except for the D3R-D4R alignment. In that case, the template was not available in the GOMoDo library[59] and thus we resorted to SWISS-MODEL[60], which also uses HHsearch[58]. Homology models were then created using MODELLER[61,62], either the version implemented in GOMoDo[59] or its standalone version (9.11). For the HR and MR models, only two models were produced for each template (default in GOMoDo). We selected the best one in terms of normalized DOPE[63] and GA341 quality values[64,65]. For the LR models, one hundred models were generated. The best one was chosen based on the same aforementioned quality criteria. No loop refinement was attempted. These models were then funneled through an information-driven molecular docking protocol using the Guru interface of the HADDOCK2.2 webserver[56]. This uses MolProbity[66] and PRODRG[67] for the setup of the protein and ligand, respectively. In addition, we predicted the putative binding cavity using Fpocket[68]. Fpocket-predicted residues whose side chains were pointing inside the receptor were used as HADDOCK active residues, whereas passive residues were automatically defined as surface neighbor residues within a 6.5 Å radius from the active residues[50]. We followed the small ligand docking protocol described in references 69 and 70. It consists of three steps. First, a rigid body docking generates 1000 initial ligand poses. Next, the best 200 poses from the previous step are refined, based on a semi-flexible simulated annealing (SA) simulation in the torsion angle space. This SA procedure consists of two cooling stages: (i) from 500 K to 50 K in 1000 MD steps and (ii) from 300 K to 50 K in 1000 MD steps. In these two stages, the ligand and the residues within 5 Å from it are allowed to move, side chains only in (i) and both side chains and backbone in (ii). Finally, three short MD simulations in explicit water refine and improve the scoring of these 200 poses: (i) heating to 100 K, 200 K and 300 K

(100 steps); (ii) 300 K simulation (1250 steps); (iii) cooling to 300 K, 200 K and 100 K (500 steps). Both ligand and protein are fully flexible, though positional restraints on the backbone heavy atoms are used to maintain the overall protein conformation. The protocol uses the recommended HADDOCK score settings for small molecules[69,70]. The obtained docking poses were then clustered based on their RMSD with a cutoff of 2.0 Å. For each cluster, the four top poses were rescored using the PRODIGY-LIG webserver[69,71]. The predicted binding energies were used to calculate the average value for each cluster. The best cluster was selected as that with the lowest average predicted binding energy.

Simulation Details

The setup of the four different systems in Table 1 was performed with in-house scripts. Four and three replicas of $hA_{2A}R$/CFF and hTAS2R16/PGP, respectively, were started using different initial velocities. The four top poses of the best cluster of the β2-AR/ADR and D3R/ETI complexes were used as the initial structures to start four different MM/CG replica simulations, each. Histidine protonation states were determined automatically using pdb2gmx[72,73], except for $hA_{2A}R$/CFF and hTAS2R16/PGP. In those cases, they were set manually in order to replicate those used in the previous Amber-based AA[39] and GROMOS-based MM/CG[29] simulations, respectively.

Our MM/CG model consists of three regions with different levels of resolution[16,17,22,23]: molecular mechanics resolution in the region around the ligand binding site (described with either the GROMOS or Amber force field), coarse-grained resolution far from the binding site (described by a Gō-like potential[21]) and a hybrid interface to connect them (see Figure 1). The definition of the MM and I regions is based on a cutoff value, calculated as the z coordinate centered between the two membrane planes ϕ_1 and ϕ_2 (Figure 1). All protein residues located above this cutoff (i.e. towards the extracellular part of the receptor) are treated at the MM level (in green color in Figure 1). The residues located up to 6 Å below the cutoff (i.e. one helical turn) form the I region (in red color in Figure 1), which is also

treated atomistically. The rest of the protein is treated at the CG level (in yellow color in Figure 1). The MM and I residues for the systems considered in this work are listed in Table S2.

The MM region was described in two ways (see Table 2):

(i) with the GROMOS 43A1 protein force field[49] together with the SPC/E water model[74]. For the CFF ligand, automatically generated PRODRG[20] parameters and charges were used. For PGP, preliminary simulations (see reference 29) showed that the automatically generated PRODRG parameterization was not able to reproduce the topology of the ligand. In particular, spurious intramolecular glucose hydrogen bonds between the 3' and 5' hydroxyl groups (see Figure S14), as well as artefactual flipping of the glucose hydroxyl groups between equatorial and axial conformations were observed. Hence, a manual procedure was used to parameterize the ligand[29]. In particular, the parameters were built by combining GROMOS 56a6_CARBO parameters[75] for the β-D-glucopyranose unit and PRODRG[20] generated parameters for the aglycon (see Figure S14). RESP charges[76] (generated using Gaussian[77] and Antechamber[78]) were used, following reference 79.

(ii) with the Amber 14SB force field[33] (taken from the GROMACS website[19]), together with the TIP3P water model[80]. Ligand parameters for CFF, PGP, ADR, and ETI were automatically generated with ACPYPE[35] using the general Amber force field (GAFF)[34] and AM1-BCC[81] charges, except for PGP, for which ligand RESP charges were taken from reference 29.

The MM/CG setup includes the introduction of five potential walls (ϕ_1 to ϕ_5, Figure 1) in order to mimic implicitly the membrane and enclose the system (see Supporting Information section *MM/CG Model* for further details). The spatial orientation of each hGPCR in the membrane, and the position of the membrane planes $\phi_{1,2}$ (mimicking the lipid polar head groups) were automatically determined by the PPM server[82]. The distance between the two membrane planes was manually adjusted so that the membrane thickness is closer to the values expected for a real membrane (35.0 Å for $hA_{2A}R$/CFF, β2-AR/ADR, and

D3R/ETI; 31.2 Å for hTAS2R16/PGP for consistency with reference 29). The potential wall ϕ_5 was built to mimic the lipid tails surrounding the protein. The system was solvated with a box of water molecules and the water molecules under the upper plane and outside of the upper hemisphere were subsequently deleted to obtain a hemispherical water droplet solvating the extracellular part of the receptor (Figure 1). This has been shown to be sufficient to ensure the proper hydration of the ligand binding site[16]. Radii of the upper and lower hemispheric walls for $hA_{2A}R$/CFF were set to 38.0 Å and 57.5 Å, respectively. The values used for the other complexes are: 50.0 Å (upper) and 50.0 Å (lower) for both β2-AR/ADR and D3R/ETI, and 53.0 Å (upper) and 35.0 Å (lower) for hTAS2R16/PGP, following reference 29. Plain cutoff schemes were used for both the electrostatic Coulomb and the van der Waals interactions, with radii 14 Å and 16 Å, respectively. No periodic boundary conditions were used and the simulations were carried out at constant temperature of 300 K. Further details on the Amber- and GROMOS-based MM/CG simulations can be found in Table 2. Specifications for the all-atom simulation of $hA_{2A}R$/CFF[39] are also shown for comparison.

An in-house MM/CG extension of GROMACS 4.5.1[72,73] was used to run the MM/CG simulations (either GROMOS- or Amber-based). The systems were first minimized and equilibrated. The equilibration procedure was system dependent. The initial structure of $hA_{2A}R$/CFF is a snapshot from an already equilibrated AA-MD simulation. Thus, only a short equilibration (5 ns with positional restraints of 1000 kJ mol^{-1} nm^{-2} on the Cα atoms) was performed. β2-AR/ADR and D3R/ETI were equilibrated for a longer time (20 ns) with positional restraints of 1000 kJ mol^{-1} nm^{-2} on the Cα atoms. hTAS2R16/PGP, based on a homology model with low sequence identity, underwent a simulated annealing procedure (from 0 K to 300 K in 6 ns, using 30 steps of 120 ps each, plus 2.4 ns at 300 K) followed by four steps (2.5 ns each) with position restraints on the Cα atoms decreasing from 1000 to 125 kJ mol^{-1} nm^{-2}.

Simulations were then continued removing all restraints and without any type of bi-

asing potential applied. The length of the simulations was 800 ns for $hA_{2A}R$/CFF and hTAS2R16/PGP, similar to previous simulations[29,39]. 500 ns were run for the β2-AR/ADR and D3R/ETI systems, where the ligands stabilized in the binding cavity in less than 100 ns, see Figures S8a to S8c. All simulations were run with a time step of 2 fs. The SHAKE algorithm was used to constrain the hydrogen bond distances. Stochastic dynamics were used to mimic water interactions to the coarse-grained part using $\tau = 0.4$ ps and $T_{\text{ref}} = 300$ K. Snapshots were written every 100 ps.

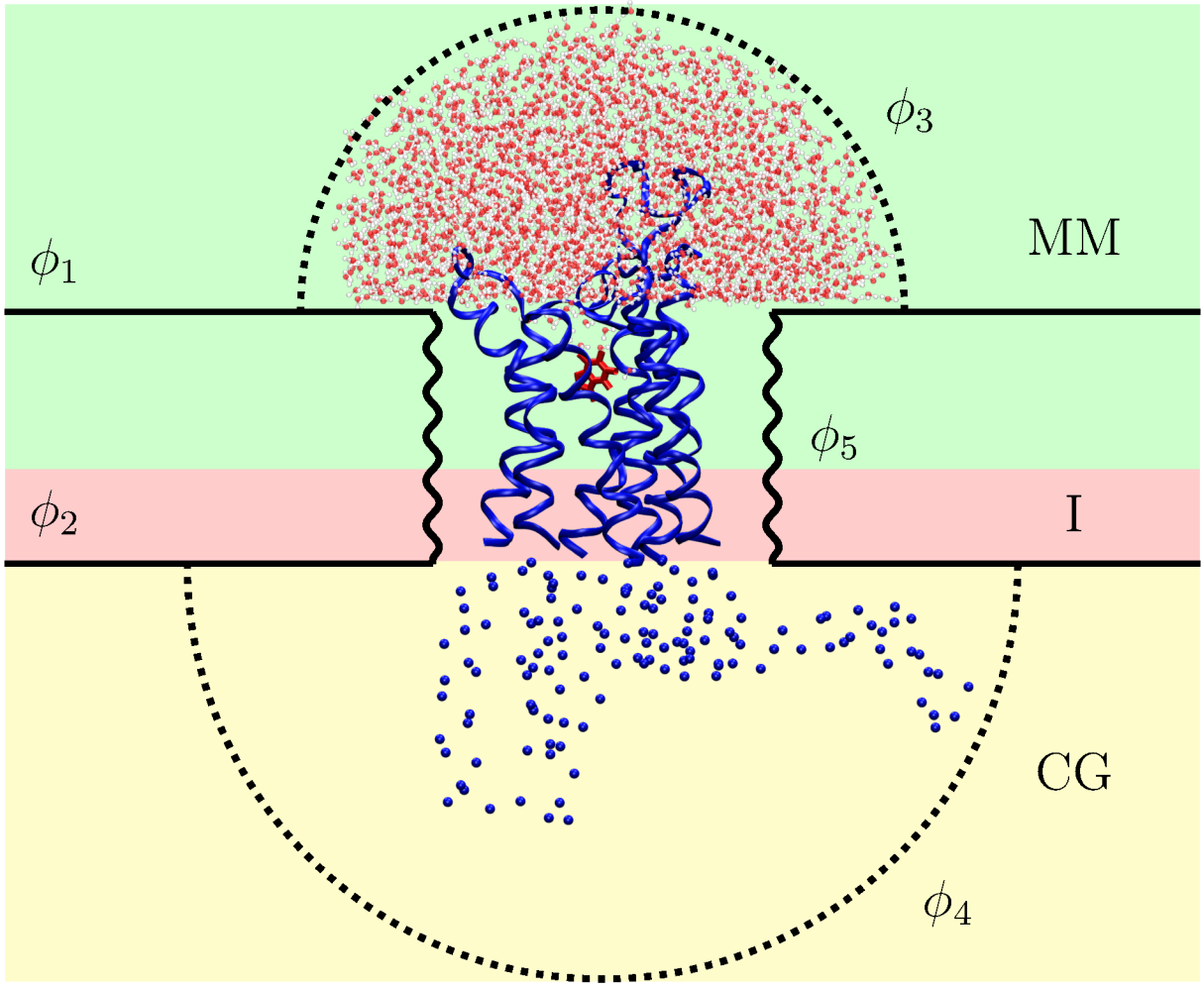

Figure 1: Typical setup of the MM/CG partitioning for a GPCR/ligand complex, using the $hA_{2A}R$/CFF system as example. The three regions (MM, I, and CG) are framed with different background colors and the potential walls (ϕ_i) are indicated with black solid lines for the planes ϕ_1 and ϕ_2, dotted lines for the hemispheres ϕ_3 and ϕ_4, and solid curly lines for ϕ_5.

Table 2: Details of the Amber- and GROMOS-based MM/CG simulations, along with the all-atom simulation of the $hA_{2A}R$/CFF system[39].

Simulation	all-atom	Amber MM/CG	GROMOS MM/CG
simulation time	800 ns	500–800 ns	800 ns
time step	2 fs	2 fs	2 fs
PBC[a]	✓	✗	✗
total atoms	≈150k	≈10k–18k	≈8k–18k
force field	Amber 99SB-ILDN	Amber 14SB	GROMOS96 43A1
ligand model	GAFF	GAFF	PRODRG[b]
ligand charges	RESP	AM1-BCC[c]	PRODRG[c]
water model	TIP3P	TIP3P	SPC/E
electrostatic cutoff	PME[d]	1.4 nm	1.4 nm
membrane	explicit	implicit (potential walls)	
ions	✓	✗	✗
thermostat	Nosé-Hoover	stochastic dynamics	
barostat	Andersen-Parrinello-Rahman	✗	✗
temperature	310 K	300 K	300 K

[a]Periodic Boundary Conditions.
[b]Following reference 29, the PGP parameters are a combination of PRODRG parameters for the phenyl aglycon and GROMOS 56a6_CARBO parameters for the glucose ring.
[c]RESP charges were used instead for PGP for consistency with reference 29.
[d]Particle Mesh Ewald.

Docking

We performed additional docking calculations for β2-AR/ADR and D3R/ETI. Besides the HADDOCK[50,56] docking to generate starting structures, Induced Fit Docking (IFD)[57] with Extended Sampling (Schrödinger-Maestro v2017-3[83]) was used. The β2-AR HR and LR models, as well as the D3R MR and LR models underwent protein preparation with the Schrödinger suite[83]. This automatically assigned bond orders for amino acid residues and protonation states of Asp, Glu, Arg, Lys, and His at pH 7.0, using the propKa code[84]. Hydrogen atoms of the resulting structures underwent geometry optimization using the OPLS3 force field[85]. Ligand preparation was performed with LigPrep[86] using the OPLS3 force

field[85]. Ligand protonation states were generated with Epik[87] using pH 7 ± 2. The most likely state at physiological conditions was chosen for each of the ligands based on the pKa values of the titrable groups (i.e. protonated amino group for both adrenaline and eticlopride). The enantiomeric states of all ligands were chosen to have the chirality of the ligands used experimentally[40,88], i.e. (-)-adrenaline and *S*-(-)-eticlopride. The docking site was enclosed in an inner box of $10 \times 10 \times 10\,\text{Å}^3$. The size of the outer box was set automatically to accommodate the docked ligands. The boxes were centered at the original position of the ligand in the crystallographic structures. The first step of the IFD[57] with extended sampling protocol is Glide docking[89] to produce initial ligand poses with two different methods, either using a softened potential or with removed side chains. Up to 80 representative poses are returned based on the GlideScore SP5.0[89] and a penalty for non-planar amide torsions. The representative poses are then used for Prime[90] side-chain prediction of residues within 5 Å of the ligand, followed by minimization of the residues and the ligand. Next, the ligand was redocked using Glide[89] with default Glide SP settings. The poses are scored with the IFD extended sampling protocol scoring function. No H-bond or core constraints were used in the docking protocol. 68, 66, 43 and 46 poses were generated for the β2-AR/ADR HR, β2-AR/ADR LR, D3R/ETI MR and D3R/ETI LR complexes, respectively.

Simulation Analysis

Ligand RMSD Analysis and Clustering

The root-mean-square deviation (RMSD) of the ligand non-hydrogen atoms was calculated using the RMSD Trajectory Tool in VMD[91] after performing least-squares-fitting of the protein Cα atoms to a reference structure. For CFF, the RMSD was determined along the entire trajectories using the last frame of the all-atom trajectory as reference. For ADR and ETI, the RMSD was calculated for the entire trajectories and representative poses obtained through clustering of the MM/CG simulations, as well as for the docking poses. The X-ray structures[40,88] were used as reference. For PGP, the ligand RMSD was calculated for

the entire trajectories and the last frame of each trajectory was the reference. The ligand RMSD analysis shows that no unbinding events occur for any of the simulations performed in this study (see Supporting Information, section *Ligand RMSD analysis* and Figures S2, S8 and S13 and Table S13).

A cluster analysis based on the RMSD of the ligand non-hydrogen atoms was performed using the GROMACS 5.1 cluster module with the gromos[92] method. In this implementation, the specified RMSD cutoff is the minimum distance of all individual structures to the cluster "central" structure. This structure can be used as the representative structure of the cluster for further analysis. The algorithm does not impose a quality threshold for the structures contained in each of the retrieved clusters. This might result in unrelated structures being classified as belonging to the same cluster[93]. To address this issue, we visualized the clusters and checked (i) for sufficient similarity across the structures within a cluster and (ii) for sufficient distance among the different clusters. RMSD cutoffs of 1.50 Å, 1.25 Å, 2.00 Å and 1.50 Å were used for CFF, PGP, ADR, and ETI, respectively. The RMSD cutoff for each system was chosen based on the distribution of ligand RMSD values across all replica simulations of the systems under consideration.

For $hA_{2A}R$/CFF, cluster analysis was performed for the last 450 ns to 800 ns of each trajectory. In the AA-MD of this complex, a receptor conformational change occurred at ≈450 ns that made the binding cavity more compact. As a result, the ligand pose changed with respect to the initial (X-ray-like) pose. Hence, the initial configuration for both the GROMOS- and Amber-based MM/CG simulations is based on a snapshot of the AA-MD taken after this receptor conformational change. The MM/CG trajectories were also analyzed only for the last 350 ns in order to have an equivalent simulation length for comparison among different simulation types. The most populated clusters, adding up to at least 90 % of the whole simulation time, were selected for further analysis.

Ligand–Receptor Interactions

Ligand–receptor interactions were determined by a combination of visual inspection of the representative structure of each cluster and automatic detection using in-house scripts (based on the HBonds tool in VMD[91] and g_mindist in GROMACS[73]). Cutoff values used to define the different types of interactions are: for hydrogen bonds, 3.5 Å donor–acceptor distance and 35° donor–hydrogen–acceptor angle (tolerance for deviation from a perfectly linear interaction); for salt bridges, 4 Å distance between charged groups; and for contacts (either hydrophobic or π-π interactions), 5.0 Å between the closest carbon atoms. Analysis of the ligand–receptor interactions using this protocol was performed for the representative structures of the most populated clusters of the MM/CG simulations, as well as for the docking poses and for the X-ray structures used for retrospective validation. Additional analyses based on the interaction persistency along the whole simulations are given in the Supporting Information (Tables S3 to S5, S7 to S12 and S14 to S16). As noted above, for the $hA_{2A}R$/CFF complex, trajectories were analyzed only for the last 350 ns. Protein residues are indicated using both the receptor sequence number and the generic class A GPCR number based on the Ballesteros-Weinstein[94] scheme (as superscript).

Comparison with experimental mutagenesis data

The agreement between simulation results and experimental mutagenesis data was quantified using the statistical parameters precision and recall[13], as well as the F_1 score. Residues for which site-directed mutagenesis data was available were classified as "experimentally binding" (EB), when their mutation increases EC_{50} or K_i values, or "experimentally non-binding" (ENB), when those values do not significantly change upon mutation. Mutagenesis data was taken from references 51 and 48 for the $hA_{2A}R$/CFF and hTAS2R16/PGP complexes, respectively. For β2-AR/ADR and D3R/ETI, mutagenesis data was retrieved from GPCRdb[1], which in turn was compiled from references 52–54 for β2-AR/ADR and reference 55 for D3R/ETI. The same residues were classified as "computationally binding" (CB)

or "computationally non-binding" (CNB) depending on the presence of the receptor–ligand interactions (hydrophobic contacts and/or direct or water-mediated H-bonds) in at least one of the representative structures of the most populated clusters.

Agreement between computational predictions and experiments results in either true positives (TP, EB+CB) or true negatives (TN, ENB+CNB). Discrepancies between computational predictions and experiments can be classified as false negatives (FN, EB+CNB) or false positives (FP, ENB+CB). The agreement was analyzed in terms of precision

$$PREC = \frac{N_{TP}}{N_{TP} + N_{FP}} \tag{1}$$

and recall

$$REC = \frac{N_{TP}}{N_{TP} + N_{FN}} \ , \tag{2}$$

where N is the number of residues of the type given in the subscript (e.g. N_{TP} is the number of residues identified as true positives), as well as their harmonic mean (F_1 score)

$$F_1 = 2 \cdot \frac{PREC \cdot REC}{PREC + REC} \ . \tag{3}$$

The first two statistical parameters indicate the agreement of the simulations with experiments, with values ranging from 0 (no agreement) to 1 (perfect agreement). F_1 measures the effectiveness of the computational predictions in retrieving accurately the experimental data. An F_1 score of 1 indicates perfect precision and recall (i.e. both low false positives and low false negatives).

Calculation of these statistical parameters may be biased because of the criteria used for the assignment of TP, FP, TN and FN. Hence, we used two alternative, yet complementary definitions of these, based (i) on the representative structures of the combined clusters or (ii) on the interaction persistency along the simulations. The use of the cluster representative structures has the limitation that these structures correspond to frames along the trajectory,

not to minimized structures, and thus do not capture the dynamical fluctuations of the protein-ligand interactions. Instead, the use of persistency values does include the intrinsic conformational fluctuations of the ligands, but, on the other hand, do not allow to pinpoint individual ligand poses. The calculated statistical parameters turn out to differ by 0.00 to 0.25. This allows us to suggest that, at least for the complexes considered here, the degree of bias related to our definitions is quite low[95].

Further analyses

To compare the receptor flexibility in the different simulations, the protein RMSF has been calculated. Details and results can be found in the Supporting Information (section *Protein RMSF analysis* and Figures S1 and S7). The *Ligand position* and the *Ligand flipping angle* have been further analysed for $A_{2A}R$/CFF and compared to the results in the publication of the all-atom simulation[39] (see the corresponding sections and Figures S3 to S6 in the Supporting Information.

Results

Amber-based MM/CG simulations were carried out on four hGPCR/ligand complexes at different resolutions: $hA_{2A}R$/CFF, β2-AR/ADR, D3R/ETI, and hTAS2R16/PGP (see Table 1). The results were validated against Amber-based AA-MD, X-ray structural data, site-directed mutagenesis experiments, GROMOS-based MM/CG simulations and docking procedures.

A high resolution model: the $hA_{2A}R$/CFF complex

Here we investigated whether the Amber-based MM/CG simulations are able to reproduce the CFF binding poses observed in the X-ray structure[38], along with an 800 ns long Amber-based AA-MD simulation by Cao et al.[39]. Comparison is also made with GROMOS-based

MM/CG simulations (Table 1).

For both GROMOS- and Amber-based MM/CG, the flexibility of the MM part of the protein (see Cα RMSF in Figure S1) is preserved relative to X-ray and all-atom MD simulations, despite the presence of the CG region.

In the Amber-based AA-MD simulation the ligand explored multiple binding poses. During the first 450 ns, CFF explores mainly a binding pose similar to the X-ray structure (see Figure S2). Afterwards, binding of a cholesterol molecule near transmembrane helix 2 changed the conformation of the receptor, making the binding cavity more compact[39]. As a result, the CFF pose changed (see Figure 2a) and this new pose remained stable for the last 350 ns of the AA-MD (see Figure S2).

For the hybrid simulations, clustering analysis on the last 350 ns (Figure 2 and Table 3) shows three representative binding poses for the Amber-based MM/CG (AM1-AM3) and four for the Gromos-based MM/CG (GM1-GM4). The two most populated clusters of the Amber-based MM/CG simulations (AM1 and AM2) are similar to those emerging from the Amber-based AA simulations[39] (AA1, see Figures 2b and 2c). The cluster AM3 (Figure 2d) has the same orientation as that of the X-ray structure[38], though displaced by about 2.5 Å further inside the receptor. We conclude that both the AA and MM/CG simulations explored additional ligand poses, besides the X-ray one. We surmise this is caused, at least in part, by two factors. On one hand, all the simulations presented here were carried out at 300 K, while the X-ray structure was solved at 200 K[96]. At higher temperatures, the ligand explores a larger number of conformations. In this regard, our results are in line with the previous AA-MD simulations (not only Amber-based[97] but also CHARMM-based[98]), and, most importantly, they are consistent with NMR experiments[97,99]. On the other, the receptor conformation present in the simulations[39] is different from the one in the initial X-ray structure[38], further influencing the binding pose. Additional details are provided in the Supporting Information (section *Discussion on the caffeine binding poses*).

The GROMOS-based MM/CG simulations sampled binding poses different from the

Amber-based all-atom and MM/CG simulations, as well as the X-ray structure. However, the most populated GROMOS-based MM/CG pose (GM1, see Figure 2e) features a similar orientation as the AM2 (Figure 2c) and AA1 poses, indicating a partial overlap between the conformational space sampled by the different simulations. Nonetheless, this pose is shifted by about 2.5 Å further inside the binding cavity, resulting in different receptor–ligand interactions (Table 3).

In addition, we validated the simulations results against mutagenesis data[51]. The Amber-based MM/CG simulations turned out to be in perfect agreement (i.e. precision, recall and F_1 score are 1.00). Instead, the agreement is lower for the GROMOS-based MM/CG (see Table 4).

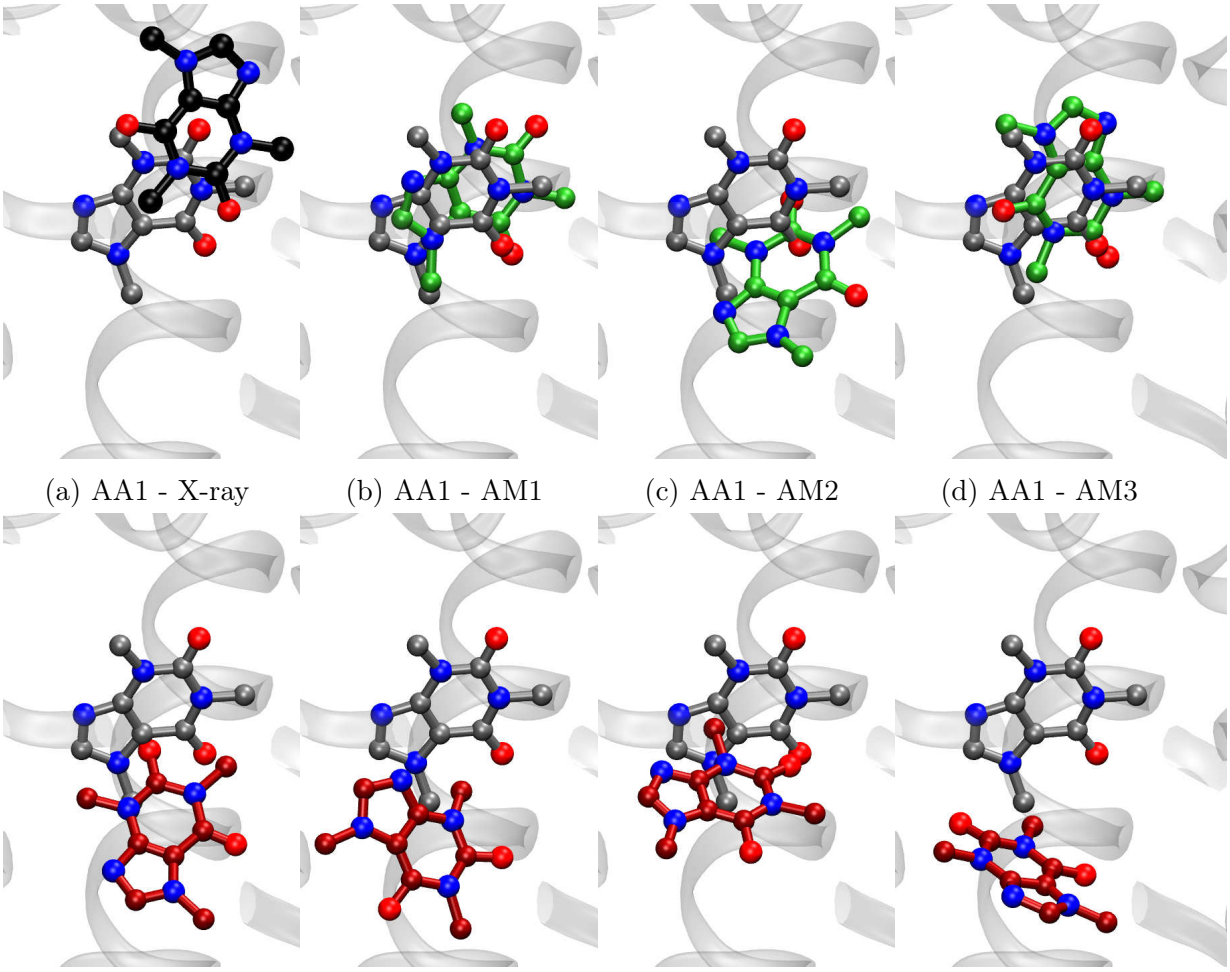

(a) AA1 - X-ray (b) AA1 - AM1 (c) AA1 - AM2 (d) AA1 - AM3

(e) AA1 - GM1 (f) AA1 - GM2 (g) AA1 - GM3 (h) AA1 - GM4

Figure 2: Representative binding poses of $hA_{2A}R$/CFF. (a) Comparison of the most populated binding pose of the reference Amber-based AA simulation (AA1, gray) with the X-ray structure (PDB code 3RFM[38], black). (b)-(d) Binding poses of the Amber (AM, green) and (e)-(h) GROMOS-based MM/CG (GM, red) simulations compared to AA1.

Table 3: Interactions of the most populated clusters for the Amber all-atom (AA), Amber-based MM/CG (AM) and GROMOS-based MM/CG (GM) simulations and the X-ray structure[38] of the $hA_{2A}R$/CFF system. The clusters are numbered consecutively according to their population, indicated as percentage. Mutagenesis data is taken from reference 51.

Residue	Interaction type	X-ray	AA1 94 %	AM1 48 %	AM2 25 %	AM3 16 %	GM1 30 %	GM2 25 %	GM3 22 %	GM4 13 %	Mutagenesis
Val55$^{2.53}$	hydrophobic	□	□	□	■	□	□	□	□	□	
Ala63$^{2.61}$	hydrophobic	□	■	■	■	■	□	□	□	□	
Ile66$^{2.64}$	hydrophobic	□	■	■	□	■	□	□	□	□	■
Ser67$^{2.65}$	H-bond	□	■	■	□	□	□	□	□	□	
Val84$^{3.32}$	hydrophobic	□	□	■	■	□	□	□	□	□	
Leu85$^{3.33}$	hydrophobic	□	■	□	■	■	■	□	□	□	■
Thr88$^{3.36}$	hydrophobic	□	■	□	■	□	□	■	□	■	
Gln89$^{3.37}$	H-bond	□	□	□	□	□	■	■	□	■	
Phe168^{ECL2}	π-stacking	■	■	■	□	■	□	□	□	□	
Met177$^{5.38}$	hydrophobic	■	□	□	■	□	□	□	□	□	■
Asn181$^{5.42}$	H-bond	□	□	□	□	□	□	□	□	■	□
Phe182$^{5.43}$	π-stacking	□	□	□	□	□	□	□	■	□	
Val186$^{5.47}$	hydrophobic	□	□	□	□	□	□	■	■	■	
Trp246$^{6.48}$	π-stacking	□	□	□	□	□	■	□	□	■	
Leu249$^{6.51}$	hydrophobic	■	■	■	■	■	■	■	□	□	
His250$^{6.52}$	H-bond	□	□	□	□	■	□	□	□	□	
	π-stacking	□	□	□	□	□	□	□	■	□	
	hydrophobic	□	■	□	□	□	□	□	□	□	
Ile252$^{6.54}$	hydrophobic	□	■	□	□	□	□	□	□	□	
Asn253$^{6.55}$	H-bond	■	□	□	□	■	■	□	□	□	■
Met270$^{7.35}$	hydrophobic	■	□	■	□	■	□	□	□	□	
Ile274$^{7.39}$	hydrophobic	■	■	■	■	■	■	□	■	□	
His278$^{7.43}$	H-bond	■	■	■	■	■	■	■	□	■	

■ direct interaction, ■ water mediated interaction and □ no interaction

Table 4: Precision ($PREC$), recall (REC) and F_1 score of the Amber- and GROMOS-based MM/CG CFF poses in $hA_{2A}R$ (see Table 3).

	Amber MM/CG	GROMOS MM/CG
$PREC$	1.00	0.67
REC	1.00	0.50
F_1	1.00	0.57

From high- to low-resolution models: the β2-AR/ADR and D3R/ETI complexes

Here, we investigated the capability of the Amber-based MM/CG approach to predict ligand binding poses starting with models of diverse resolution. We focused on two complexes (β2-AR/ADR and D3R/ETI) and generated two models at different resolution for each of them (see Table 1).

For both receptors, the Cα RMSF values calculated from the Amber-based MM/CG simulations compare well with those from CHARMM-based AA-MD[100] (Figure S7), as well as with the crystallographic β-factors[40,88] (see Supporting Information for details).

For β2-AR/ADR, the X-ray structure[40] shows that the ligand forms a salt bridge with Asp113$^{3.32}$ (conserved across aminergic receptors[44,101]) and H-bonds with Asp113$^{3.32}$, Ser203$^{5.42}$, Ser207$^{5.46}$, Asn293$^{6.55}$, and Asn312$^{7.39}$ (the last is conserved across β-adrenergic receptors[44]).

The Amber-based MM/CG simulation of β2-AR/ADR (HR) reproduces all of the crystallographic interactions[40] (see Table 5). This contrasts with the HADDOCK or IFD-based dockings started from the same receptor model. These docking approaches reproduced the salt bridge with Asp113$^{3.32}$, but they missed some of the H-bonds.

As expected, the predictive power turned out to be lower in the LR model (see Table 5). The Amber-based MM/CG-derived simulations and IFD predicted interactions with residues Asp113$^{3.32}$, Asn293$^{6.55}$ and Asn312$^{7.39}$, but missed two H-bonds with Ser203$^{5.42}$ and Ser207$^{5.46}$. The HADDOCK docking poses missed most interactions, in particular the H-

bond with Asp113$^{3.32}$.

In addition, the Amber-based MM/CG simulations predict a hydrogen bond with Ser204$^{5.43}$, either direct for the HR model or water-mediated for the LR model. The crystallographic pose is compatible with the presence of a water-mediated hydrogen bond with Ser204$^{5.43}$[40].

Mutagenesis data for the β2-AR/ADR complex[1,52,54,102,103] (see last column in Table 5) suggests that Ser203$^{5.42}$, Ser204$^{5.43}$, Asn293$^{6.55}$, and Asn312$^{7.39}$ are involved in binding (EB, see *Methods*), while Cys116$^{3.35}$ is not (ENB). Validation of the Amber-based MM/CG simulations against this data shows that precision is maximal, while recall and F_1 score are higher compared to docking (Table 6).

In addition, we compared the Amber-based MM/CG results with CHARMM-based AA-MD studies previously published in the literature. In the case of the β2-AR/ADR complex, the ligand RMSD values (Table S13) were comparable to those previously reported for the AA-MD[104]. Furthermore, the receptor–ligand interactions also agree with AA-MD simulations[105,106].

For D3R/ETI, the X-ray structure[88] shows that the tertiary amine of the ligand five-membered ring, positively charged at physiological pH (see Figure S10), forms a salt-bridge with Asp110$^{3.32}$. Furthermore, the aromatic ring of eticlopride interacts with a hydrophobic pocket composed by residues Val111$^{3.33}$, Ile183^{ECL2}, Val189$^{5.39}$, Phe345$^{6.51}$, Phe346$^{6.52}$.

The MR Amber-based MM/CG reproduced all of the crystallographic interactions, while the LR appeared to miss the hydrogen bonds with His349$^{6.55}$ and Tyr365$^{7.35}$ (see Table 7). However, it should be noted that these two hydrogen bonds are only present in one of the two chains (A) of the X-ray structure (PDB code 3PBL). Instead, in the other chain (B), His349$^{6.55}$ does not interact with the ligand, whereas Tyr365$^{7.35}$ interacts only indirectly through Phe345$^{6.51}$. Therefore, the simulation results are still compatible with the crystallographic interactions. The Amber-based MM/CG seemed to be more successful at predicting receptor–ligand interactions than docking alone for the same receptor model, either MR or LR (Table 7).

This comparison with the X-ray structure was also complemented by validation against mutagenesis data[1,55]. Based on the change in K_i upon mutation (see *Methods*), Tyr365$^{7.35}$, Ile183^{ECL2}, Val189$^{5.39}$, and Tyr373$^{7.43}$ were classified as EB residues, and Ser182^{ECL2} as ENB (see last column of Table 7). The precision was 1.00 for most computational approaches, including MM/CG. However, in most cases the recall and F_1 score were higher for MM/CG than docking (Table 8).

For D3R/ETI, ligand RMSD values obtained in our Amber-based MM/CG simulations (Table S13) are comparable to those of a CHARMM-based AA-MD simulation[55]. Amber-based MM/CG simulations recovered the interactions with Asp110$^{3.32}$ and His349$^{6.55}$ (Table 7), in line with a CHARMM-based AA-MD[107].

To complement the comparison of the ligand poses for β2-AR/ADR and D3R/ETI, the superimposition of the X-ray poses with the cluster representatives emerging from the Amber-based simulations and the HADDOCK poses can be found in the Supporting Information (Figures S11 and S12).

Table 5: β2-AR/ADR interactions predicted using different receptor models[a] and computational approaches[b]. Retrospective validation is performed by comparison with experimental data[c].

Residue	Interaction type	X-ray	HR MM/CG	LR MM/CG	HR HADDOCK	LR HADDOCK	HR IFD	LR IFD	Mutagenesis
Asp113$^{3.32}$	Salt-bridge (N^+)	■	■	■	■	■	■	■	
Asp113$^{3.32}$	H-bond (tail OH)	■	■	■	□	□	■	■	
Ser203$^{5.42}$	H-bond	■	■	□	■	■	■	□	■
Ser204$^{5.43}$	H-bond	■	■	■	□	■	□	□	■
Ser207$^{5.46}$	H-bond	■	■	□	■	■	□	□	
Asn293$^{6.55}$	H-bond	■	■	■	□	□	■	■	■
Asn312$^{7.39}$	H-bond (N^+)	■	■	□	■	□	■	□	■
Asn312$^{7.39}$	H-bond (tail OH)	■	■	■	□	□	■	■	■
Trp109$^{3.28}$	contact	■	■	■	■	■	■	□	
Cys116$^{3.35}$	contact	□	□	□	□	□	□	□	□
Val117$^{3.36}$	contact	■	■	■	■	■	■	■	
Phe193^{ECL2}	contact	■	□	■	□	■	□	■	
Ser207$^{5.46}$	contact	■	■	■	■	■	■	□	
Trp286$^{6.48}$	contact	■	■	■	■	■	■	■	
Phe289$^{6.51}$	contact	■	■	■	■	■	■	■	
Phe290$^{6.52}$	contact	■	■	■	■	■	■	■	
Tyr308$^{7.35}$	contact	■	■	■	■	■	■	■	
Tyr316$^{7.43}$	contact	■	■	■	■	■	□	■	

■ direct interaction, ■ water mediated interaction and □ no interaction

[a]high (HR) and low (LR) resolution models, see Table 1.
[b]Amber-based MM/CG simulations and HADDOCK and IFD dockings.
[c]X-ray structure (PDB code 4LDO)[40] and mutagenesis data[1,52,54,102,103].

Table 6: Precision ($PREC$), recall (REC), and F_1 score for the β2-AR/ADR complex computational predictions (see Table 5).

	HR MM/CG	LR MM/CG	HR HADDOCK	LR HADDOCK	HR IFD	LR IFD
$PREC$	1.00	1.00	1.00	1.00	1.00	1.00
REC	1.00	0.60	0.40	0.40	0.80	0.40
F_1	1.00	0.75	0.57	0.57	0.89	0.57

Table 7: D3R/ETI interactions predicted using different receptor models[a] and computational approaches[b]. Retrospective validation is performed by comparison with experimental data[c].

Residue	Interaction type	X-ray	MR MM/CG	LR MM/CG	MR HADDOCK	LR HADDOCK	MR IFD	LR IFD	Mutagenesis
Asp110$^{3.32}$	Salt-bridge	■	■	■	■	■	□	■	
Ser182^{ECL2}	H-bond	□	□	□	□	□	■	□	□
His349$^{6.55}$	H-bond*	■	■	□	□	□	□	■	
Tyr365$^{7.35}$	H-bond**	■	■	□	□	□	□	□	■
Val86$^{2.61}$	contact	■	■	■	■	■	■	■	
Phe106$^{3.28}$	contact	■	■	■	■	■	■	■	
Val107$^{3.29}$	contact	■	■	■	■	□	■	■	
Val111$^{3.33}$	contact	■	■	■	■	■	■	■	
Thr115$^{3.37}$	contact	■	■	■	■	■	■	□	
Ile183^{ECL2}	contact	■	■	■	■	■	■	■	■
Val189$^{5.39}$	contact	■	■	■	■	■	■	□	■
Ser192$^{5.42}$	contact	■	■	■	■	■	■	□	
Ser193$^{5.43}$	contact	■	■	■	■	■	■	□	
Ser196$^{5.46}$	contact	■	■	■	■	■	■	□	
Trp342$^{6.48}$	contact	■	■	■	■	■	■	■	
Phe345$^{6.51}$	contact	■	■	■	■	■	■	■	
Phe346$^{6.52}$	contact	■	■	■	■	■	■	■	
Val350$^{6.56}$	contact	■	■	□	■	□	□	□	
Tyr373$^{7.43}$	contact	■	■	■	■	■	■	■	■

■ direct interaction, ■ water mediated interaction and □ no interaction
*H-bond only present in one out of the two chains in the PDB
**putative water-mediated H-bond only possible in one out of the two chains in the PDB

[a]medium (MR) and low (LR) resolution models, see Table 1.
[b]Amber-based MM/CG simulations and HADDOCK and IFD dockings.
[c]X-ray structure (PDB code 3PBL)[88] and mutagenesis data[1,55].

Table 8: Precision ($PREC$), recall (REC), and F_1 score for the D3R/ETI complex computational predictions (see Table 7).

	MR MM/CG	LR MM/CG	MR HADDOCK	LR HADDOCK	MR IFD	LR IFD
$PREC$	1.00	1.00	1.00	1.00	0.75	1.00
REC	1.00	0.75	0.75	0.75	0.75	0.50
F_1	1.00	0.86	0.86	0.86	0.75	0.67

Low resolution model: hTAS2R16/PGP complex

For bitter taste receptors, experimental structural information is lacking and the best templates for homology modeling show a sequence identity of only 15 %. Therefore, the only experimental data available to validate these simulations consists of *in vitro* functional assays of receptor mutants[48]. Based on the experimental data for hTAS2R16, residues Glu86$^{3.36}$, Asn89$^{3.39}$, Phe93$^{3.40}$, His181$^{5.43}$, Phe240$^{6.52}$ and Ile243$^{6.55}$ are important for ligand binding in this receptor, whereas Gln177$^{5.39}$ is not[29] (see Table 9).

Here we compared the GROMOS-based MM/CG simulation of the hTAS2R16/PGP complex carried out by Fierro et al.[29] with Amber-based MM/CG simulations (this work). Our aim was to assess the performance of the two MM/CG implementations for such low resolution cases with limited experimental data for validation.

Both Amber- and GROMOS-based MM/CG simulations maintained hydrogen bonds to Glu86$^{3.36}$ and Asn89$^{3.39}$, as well as a second shell H-bond with His181$^{5.43}$, but did not identify interactions with Ile243$^{6.55}$, consistent with mutagenesis data. However, Amber-based MM/CG sampled hydrophobic and/or second shell π-stacking interactions with Phe93$^{3.40}$ and Phe240$^{6.52}$ (two residues experimentally verified as involved in binding), whereas these interactions are only present in one GROMOS-based MM/CG cluster. Furthermore, GROMOS-based MM/CG predicted a H-bond with Gln177$^{5.39}$, while Amber-based MM/CG correctly determined this residue as non-binding (see Figure S15 and Table 9). As a result, Amber MM/CG featured better precision and F_1 score and similar recall compared to the

GROMOS-based MM/CG simulation in reference 29. Nonetheless, both hybrid simulations showed better statistical values than docking[29] (Table 10).

Table 9: Interactions of the most populated clusters for the Amber- (AM) and GROMOS-based MM/CG (GM) simulations of the hTAS2R16/PGP system compared to mutagenesis data[48]. The clusters are numbered consecutively according to their population, indicated as percentage.

Residue	Interaction type	Mutagenesis	AM combined	GM combined	AM1 48 %	AM2 23 %	AM3 13 %	GM1 44 %	GM2 23 %	GM3 10 %	GM4 7 %
Glu86$^{3.36}$	H-bond	■	■	■	■	■	■	■	■	■	■
Asn89$^{3.39}$	H-bond	■	■	■	■	■	■	■	■	■	□
Phe93$^{3.40}$	hydrophobic/ 2nd shell π-stacking	■	■	■	■	■	■	□	■	□	□
Gln177$^{5.39}$	H-bond	□	□	■	□	□	□	■	■	□	■
His181$^{5.43}$	2nd shell H-bond	■	■	■	■	■	■	■	■	■	□
Phe240$^{6.52}$	2nd shell π-stacking	■	■	■	■	■	■	□	■	□	□
Ile243$^{6.55}$	unknown	■	□	□	□	□	□	□	□	□	□

■ direct interaction, ■ water mediated interaction and □ no interaction

Table 10: Precision ($PREC$), recall (REC), and F_1 score of the Amber- and GROMOS-based MM/CG PGP poses in hTAS2R16 (see Table 9). Results for docking taken from reference 29.

	Amber MM/CG	GROMOS MM/CG	HADDOCK
$PREC$	1.00	0.83	0.50
REC	0.83	0.83	0.50
F_1	0.91	0.83	0.50

Discussion

In this work, we introduced the Amber force field into our existing MM/CG interface, based on the GROMACS code[72,73]. The MM part of the code can now be described either with a united-atom force field (GROMOS96 43A1, PRODRG and SPC/E for the protein, lig-

and, and water, respectively) or with an all-atom force field (i.e. Amber ff14SB, GAFF and TIP3P). The MM/CG setup was simplified by replacing the use of an external webserver (PRODRG[20]) with a program (ACPYPE[35]) fully integrated into the ligand parameterization workflow. ACPYPE automatically provides small molecule parameters, using GAFF and AM1-BCC charges, that are consistent with the Amber all-atom protein force field[81]. Therefore, simulation of ligand–receptor complexes is possible without the need of a long manual ligand parameterization procedure.

The predictive power of the Amber MM/CG was tested in four hGPCR/ligand complexes using models at different resolutions (see Table 1). The Amber-based MM/CG simulations of $hA_{2A}R$/CFF (HR) turned out to be in good agreement with AA-MD and X-ray. The prediction was better than that made with the GROMOS MM/CG. One possible cause may be the limited compatibility of the PRODRG charges with the GROMOS force field, as already pointed out by Lemkul et al.[79]. In addition, the Amber-based MM/CG simulations of both $hA_{2A}R$/CFF (HR) and hTAS2R16/PGP (LR) showed better agreement with mutagenesis and functional data than GROMOS-based MM/CG. Therefore, the Amber force field performed significantly better at describing the receptor–ligand interactions than GROMOS-based MM/CG.

The Amber MM/CG approach was validated retrospectively by using two additional hGPCR/ligand complexes, β2-AR/ADR and D3R/ETI, for which a wealth of experimental data is available (Table 1). The Amber-based MM/CG approach reproduced the ligand poses observed in the X-ray structures[40,88] and the predicted binding residues agree with the mutagenesis data. The Amber-based MM/CG of β2-AR/ADR (HR) and D3R/ETI (MR) reproduced well the crystallographic interactions. For the LR models, the Amber-based MM/CG was still able to predict overall correct binding poses and recover most of the X-ray receptor–ligand interactions. Comparison with previous AA-MD simulations also showed a good agreement.

The Amber-based MM/CG simulations for both β2-AR/ADR and D3R/ETI reproduce

better the X-ray receptor–ligand interactions than docking (especially for the LR models). They perform better in recovering binding residues predicted by mutagenesis (recall) and similarly in distinguishing binding from non-binding residues (precision). This is in line with previous studies suggesting molecular simulations for refining docking poses in homology models[108].

Furthermore, the MM/CG simulations revealed the presence of water mediated hydrogen bonds, which were not evident in the X-ray structure (where water molecules were not resolved) and/or docking poses. For $hA_{2A}R$/CFF, AA-MD, as well as both MM/CG simulations (GROMOS- and Amber-based), revealed a water-mediated hydrogen bond with His278$^{7.43}$. Retrospective visualization of the X-ray structure shows that such water-mediated interaction can also be possible in the crystal structure[38]. In the β2-AR/ADR complex, a water-mediated hydrogen bond between the catechol group of the ligand and Ser204$^{5.43}$ can also be proposed based on the findings in the MM/CG simulations. Interestingly, such interaction might also provide a rationale for the change in K_i observed experimentally upon mutation of this residue[54,109].

Conclusions

We have presented an implementation of the Amber MM/CG scheme, tailored to predict ligand poses to hGPCRs. The implementation was tested by running more than 13 µs of Amber-based MM/CG simulations on a variety of complexes at different resolution, based on X-ray structures, AA-MD simulation snapshots and homology models. The simulations were validated retrospectively using X-ray structures and all-atom MD simulations, as well as site-directed mutagenesis data. Comparison with docking poses was also made. The Amber MM/CG approach turned out to recover the crystallographically observed receptor–ligand contacts. This is particularly useful for LR models, for which docking alone can miss some interactions due to the limited accuracy of side chain predictions.

We expect our approach to be applicable to the prediction of ligand binding poses in other GPCRs, regardless of the resolution of available structural information (X-ray or cryo-EM experimental structures, AA-MD simulations, or homology models). Amber-based MM/CG simulations might reveal themselves as a useful tool for predicting ligand poses in low-resolution homology models[110,111] and low-affinity complexes[98,112,113], or to predict water-mediated ligand contacts. Although AA-MD can also be used for HR or MR models[114–117], the MM/CG approach is less computationally expensive.

The Amber MM/CG approach could also be applied for virtual ligand screening, by running multiple simulations of the same receptor bound to different ligands simultaneously. The MM/CG setup involves one order of magnitude less atoms than a fully atomistic system (see Table 2). As a result, the MM/CG simulation of $hA_{2A}R$/CFF is approximately one order of magnitude faster than the corresponding all-atom MD simulation when using two 3 GHz processors. Besides predicting ligand poses, the Amber MM/CG approach, together with the recently developed open boundary (OB-)MM/CG for grand canonical simulations[118], could be used to calculate ligand binding free energies. Indeed, the OB-MM/CG improves the description of the structural and dynamical properties of water[118], thus enabling a rigorous implementation of free energy methods. The MM/CG code is freely available on the Hybrid MM/CG webserver (`https://mmcg.grs.kfa-juelich.de/`; see the Download section)[119].

Acknowledgement

The authors thank Dr. Vania Calandrini, Dr. Emiliano Ippoliti and Dr. Thomas Tarenzi for their support regarding the setup of the MM/CG simulations, as well as Dr. Fabrizio Fierro for providing access to his GROMOS-based MM/CG trajectories of the hTAS2R16/PGP system and useful discussions. Simulations were performed with computing resources granted by RWTH Aachen University under project jara0165. Paolo Carloni and Mercedes Alfonso-Prieto also thank the financial support of the "Ernesto Illy Foundation" (Trieste, Italy).

Paolo Carloni received funding from the EBRAINS research infrastructure, funded from the European Union's Horizon 2020 294 Framework Programme for Research and Innovation under the Specific Grant Agreement No. 945539295 (Human Brain Project SGA3).

Associated Content

Supporting Information Available: Further details on the MM/CG scheme, additional analyses and discussions of the $hA_{2A}R$/CFF complex (protein RMSF, ligand RMSD, position, flipping angle, protein–ligand hydrogen bonds and contacts, comparison with mutagenesis data, and binding pose discussion), the β2-AR/ADR and D3R/ETI complexes (protein RMSF, ligand RMSD, protein–ligand hydrogen bonds and contacts, comparison with mutagenesis data, and ligand superimpositions with X-ray), and the hTAS2R16/PGP complex (ligand RMSD, protein–ligand hydrogen bonds and contacts, comparison with mutagenesis data, and ligand superimpositions).

References

(1) Pándy-Szekeres, G.; Munk, C.; Tsonkov, T. M.; Mordalski, S.; Harpsøe, K.; Hauser, A. S.; Bojarski, A. J.; Gloriam, D. E. GPCRdb in 2018: adding GPCR structure models and ligands. *Nucleic Acids Res* **2017**, *46*, D440–D446.

(2) Hauser, A. S.; Chavali, S.; Masuho, I.; Jahn, L. J.; Martemyanov, K. A.; Gloriam, D. E.; Babu, M. M. Pharmacogenomics of GPCR drug targets. *Cell* **2018**, *172*, 41–54.

(3) Hauser, A. S.; Attwood, M. M.; Rask-Andersen, M.; Schiöth, H. B.; Gloriam, D. E. Trends in GPCR drug discovery: new agents, targets and indications. *Nat Rev Drug Discov* **2017**, *16*, 829.

(4) Di Pizio, A.; Behrens, M.; Krautwurst, D. Beyond the flavour: the potential druggability of chemosensory G Protein-Coupled receptors. *Int J Mol Sci* **2019**, *20*, 1402.

(5) Lee, S.-J.; Depoortere, I.; Hatt, H. Therapeutic potential of ectopic olfactory and taste receptors. *Nat Rev Drug Discov* **2019**, *18*, 116–138.

(6) Basith, S.; Cui, M.; Macalino, S. J. Y.; Park, J.; Clavio, N. A. B.; Kang, S.; Choi, S. Exploring G Protein-Coupled Receptors (GPCRs) Ligand Space via Cheminformatics Approaches: Impact on Rational Drug Design. *Front Pharmacol* **2018**, *9*, 128.

(7) GPCRdb. `http://gpcrdb.org`, [Online; accessed January 31st 2020].

(8) Munk, C.; Mutt, E.; Isberg, V.; Nikolajsen, L. F.; Bibbe, J. M.; Flock, T.; Hanson, M. A.; Stevens, R. C.; Deupi, X.; Gloriam, D. E. An online resource for GPCR structure determination and analysis. *Nat Methods* **2019**, *16*, 151–162.

(9) Kufareva, I.; Katritch, V.; Stevens, R. C.; Abagyan, R. Advances in GPCR modeling evaluated by the GPCR Dock 2013 assessment: meeting new challenges. *Structure* **2014**, *22*, 1120–1139.

(10) Cavasotto, C. N.; Palomba, D. Expanding the horizons of G protein-coupled receptor structure-based ligand discovery and optimization using homology models. *ChemComm* **2015**, *51*, 13576–13594.

(11) Esguerra, M.; Siretskiy, A.; Bello, X.; Sallander, J.; Gutiérrez-de Terán, H. GPCR-ModSim: A comprehensive web based solution for modeling G-protein coupled receptors. *Nucleic Acids Res* **2016**, *44*, W455–W462.

(12) Heifetz, A.; James, T.; Morao, I.; Bodkin, M. J.; Biggin, P. C. Guiding lead optimization with GPCR structure modeling and molecular dynamics. *Curr Opin Pharmacol* **2016**, *30*, 14–21.

(13) Fierro, F.; Suku, E.; Alfonso-Prieto, M.; Giorgetti, A.; Cichon, S.; Carloni, P. Agonist Binding to Chemosensory Receptors: A Systematic Bioinformatics Analysis. *Front Mol Biosci* **2017**, *4*, 63.

(14) Lupala, C. S.; Rasaeifar, B.; Gomez-Gutierrez, P.; Perez, J. J. Using molecular dynamics for the refinement of atomistic models of GPCRs by homology modeling. *J Biomol Struct Dyn* **2018**, *36*, 2436–2448.

(15) Rodríguez-Espigares, I.; Torrens-Fontanals, M.; Tiemann, J. K.; Aranda-García, D.; Ramírez-Anguita, J. M.; Stepniewski, T. M.; Worp, N.; Varela-Rial, A.; Morales-Pastor, A.; Lacruz, B. M.; Pándy-Szekeres, G.; Mayol, E.; Giorgino, T.; Carlsson, J.; Deupi, X.; Filipek, S.; Filizola, M.; Gómez-Tamayo, J. C.; Gonzalez, A.; Gutierrez-de Teran, H.; Jimenez, M.; Jespers, W.; Kapla, J.; Khelashvili, G.; Kolb, P.; Latek, D.; Marti-Solano, M.; Matricon, P.; Matsoukas, M.-T.; Miszta, P.; Olivella, M.; Perez-Benito, L.; Provasi, D.; Ríos, S.; Rodríguez-Torrecillas, I.; Sallander, J.; Sztyler, A.; Vaidehi, N.; Vasile, S.; Weinstein, H.; Zachariae, U.; Hildebrand, P. W.; Fabritiis, G. D.; Sanz, F.; Gloriam, D. E.; Cordomí, A.; Guixà-González, R.; Selent, J. GPCRmd uncovers the dynamics of the 3D-GPCRome. *bioRxiv* **2019**, 839597.

(16) Leguèbe, M.; Nguyen, C.; Capece, L.; Hoang, Z.; Giorgetti, A.; Carloni, P. Hybrid Molecular Mechanics/Coarse-Grained Simulations for Structural Prediction of G-Protein Coupled Receptor/Ligand Complexes. *PLOS ONE* **2012**, *7*, e47332.

(17) Schneider, J.; Korshunova, K.; Musiani, F.; Alfonso-Prieto, M.; Giorgetti, A.; Carloni, P. Predicting ligand binding poses for low-resolution membrane protein models: Perspectives from multiscale simulations. *Biochem Biophys Res Commun* **2018**, *498*, 366–374.

(18) Alfonso-Prieto, M.; Navarini, L.; Carloni, P. Understanding ligand binding to G-protein coupled receptors using multiscale simulations. *Front Mol Biosci* **2019**, *6*.

(19) GROMACS: Force fields. `http://www.gromacs.org/Downloads/User_contributions/Force_fields`, [Online; accessed January 31st 2020].

(20) Schüttelkopf, A. W.; van Aalten, D. M. F. PRODRG: a tool for high-throughput crystallography of protein-ligand complexes. *Acta Crystallogr* **2004**, *D60*, 1355–1363.

(21) Gō, N.; Abe, H. Noninteracting local-structure model of folding and unfolding transition in globular proteins. I. Formulation. *Biopolymers* **1981**, *20*, 991–1011.

(22) Neri, M.; Anselmi, C.; Cascella, M.; Maritan, A.; Carloni, P. Coarse-Grained Model of Proteins Incorporating Atomistic Detail of the Active Site. *Phys Rev Lett* **2005**, *95*, 218102.

(23) Neri, M.; Baaden, M.; Carnevale, V.; Anselmi, C.; Maritan, A.; Carloni, P. Microseconds dynamics simulations of the outer-membrane protease T. *Biophys J* **2008**, *94*, 71–78.

(24) Punta, M.; Forrest, L. R.; Bigelow, H.; Kernytsky, A.; Liu, J.; Rost, B. Membrane protein prediction methods. *Methods* **2007**, *41*, 460–474.

(25) Piccoli, S.; Suku, E.; Garonzi, M.; Giorgetti, A. Genome-wide membrane protein structure prediction. *Curr Genom* **2013**, *14*, 324–329.

(26) Olivella, M.; Gonzalez, A.; Pardo, L.; Deupi, X. Relation between sequence and structure in membrane proteins. *Bioinformatics* **2013**, *29*, 1589–1592.

(27) Marchiori, A.; Capece, L.; Giorgetti, A.; Gasparini, P.; Behrens, M.; Carloni, P.; Meyerhof, W. Coarse-grained/molecular mechanics of the TAS2R38 bitter taste receptor: experimentally-validated detailed structural prediction of agonist binding. *PLOS ONE* **2013**, *8*, e64675.

(28) Sandal, M.; Behrens, M.; Brockhoff, A.; Musiani, F.; Giorgetti, A.; Carloni, P.; Meyerhof, W. Evidence for a Transient Additional Ligand Binding Site in the TAS2R46 Bitter Taste Receptor. *J Chem Theory Comput* **2015**, *11*, 4439–4449.

(29) Fierro, F.; Giorgetti, A.; Carloni, P.; Meyerhof, W.; Alfonso-Prieto, M. Dual binding mode of "bitter sugars" to their human bitter taste receptor target. *Sci Rep* **2019**, *9*, 8437.

(30) Capaldi, S.; Suku, E.; Antolini, M.; Di Giacobbe, M.; Giorgetti, A.; Buffelli, M. Allosteric sodium binding cavity in GPR3: a novel player in modulation of Aβ production. *Sci Rep* **2018**, *8*, 1–11.

(31) Cherezov, V.; Rosenbaum, D. M.; Hanson, M. A.; Rasmussen, S. G. F.; Thian, F. S.; Kobilka, T. S.; Choi, H.-J.; Kuhn, P.; Weis, W. I.; Kobilka, B. K.; Stevens, R. C. High-resolution crystal structure of an engineered human β2-adrenergic G protein–coupled receptor. *Science* **2007**, *318*, 1258–1265.

(32) Vanni, S.; Neri, M.; Tavernelli, I.; Rothlisberger, U. Predicting novel binding modes of agonists to β adrenergic receptors using all-atom molecular dynamics simulations. *PLoS Comput Biol* **2011**, *7*, e1001053.

(33) Maier, J. A.; Martinez, C.; Kasavajhala, K.; Wickstrom, L.; Hauser, K. E.; Simmerling, C. ff14SB: improving the accuracy of protein side chain and backbone parameters from ff99SB. *J Chem Theory Comput* **2015**, *11*, 3696–3713.

(34) Wang, J.; Wolf, R. M.; Caldwell, J. W.; Kollman, P. A.; Case, D. A. Development and testing of a general amber force field. *J Comput Chem* **2004**, *25*, 1157–1174.

(35) da Silva, A. W. S.; Vranken, W. F. ACPYPE-Antechamber python parser interface. *BMC Res Notes* **2012**, *5*, 367.

(36) Michino, M.; Abola, E.; Brooks, C. L.; Dixon, J. S.; Moult, J.; Stevens, R. C. Community-wide assessment of GPCR structure modelling and ligand docking: GPCR Dock 2008. *Nature Reviews Drug Discovery* **2009**, *8*, 455–463.

(37) Kufareva, I.; Rueda, M.; Katritch, V.; Stevens, R.; Abagyan, R. Status of GPCR modeling and docking as reflected by community-wide GPCR Dock 2010 assessment. *Structure* **2011**, *19*, 1108–1126.

(38) Doré, A. S.; Robertson, N.; Errey, J. C.; Ng, I.; Hollenstein, K.; Tehan, B.; Hurrell, E.; Bennett, K.; Congreve, M.; Magnani, F.; Tate, C. G.; Weir, M.; Marshall, F. H. Structure of the Adenosine A2A Receptor in Complex with ZM241385 and the Xanthines XAC and Caffeine. *Structure* **2011**, *19*, 1283–1293.

(39) Cao, R.; Rossetti, G.; Bauer, A.; Paolo, C. Binding of the Antagonist Caffeine to the Human Adenosine Receptor hA2AR in Nearly Physiological Conditions. *PLOS ONE* **2015**, *10*, e0126833.

(40) Ring, A. M.; Manglik, A.; Kruse, A. C.; Enos, M. D.; Weis, W. I.; Garcia, K. C.; Kobilka, B. K. Adrenaline-activated structure of β 2-adrenoceptor stabilized by an engineered nanobody. *Nature* **2013**, *502*, 575–579.

(41) Material in the Supporting Information is organized based on the GPCR/ligand systems studied in this work. As a result, supporting figures and tables are not numbered following the order they appear in the main text.

(42) Kruse, A. C.; Ring, A. M.; Manglik, A.; Hu, J.; Hu, K.; Eitel, K.; Hübner, H.; Pardon, E.; Valant, C.; Sexton, P. M.; Christopoulos, A.; Felder, C. C.; Gmeiner, P.; Steyaert, J.; Weis, W. I.; Garcia, K. C.; Wess, J.; Kobilka, B. K. Activation and allosteric modulation of a muscarinic acetylcholine receptor. *Nature* **2013**, *504*, 101–106.

(43) Costanzi, S.; Cohen, A.; Danfora, A.; Dolatmoradi, M. Influence of the Structural Accuracy of Homology Models on Their Applicability to Docking-Based Virtual Screening: The β2 Adrenergic Receptor as a Case Study. *J Chem Inf Model* **2019**, *59*, 3177–3190.

(44) Michino, M.; Beuming, T.; Donthamsetti, P.; Newman, A. H.; Javitch, J. A.; Shi, L. What can crystal structures of aminergic receptors tell us about designing subtype-selective ligands? *Pharmacol Rev* **2015**, *67*, 198–213.

(45) Wang, S.; Wacker, D.; Levit, A.; Che, T.; Betz, R. M.; McCorvy, J. D.; Venkatakrishnan, A. J.; Huang, X.-P.; Dror, R. O.; Shoichet, B. K.; Roth, B. L. D4 dopamine receptor high-resolution structures enable the discovery of selective agonists. *Science* **2017**, *358*, 381–386.

(46) Beuming, T.; Sherman, W. Current assessment of docking into GPCR crystal structures and homology models: successes, challenges, and guidelines. *J Chem Inf Model* **2012**, *52*, 3263–3277.

(47) Haga, K.; Kruse, A. C.; Asada, H.; Yurugi-Kobayashi, T.; Shiroishi, M.; Zhang, C.; Weis, W. I.; Okada, T.; Kobilka, B. K.; Haga, T.; Kobayashi, T. Structure of the human M2 muscarinic acetylcholine receptor bound to an antagonist. *Nature* **2012**, *482*, 547–551.

(48) Sakurai, T.; Misaka, T.; Ishiguro, M.; Masuda, K.; Sugawara, T.; Ito, K.; Kobayashi, T.; Matsuo, S.; Ishimaru, Y.; Asakura, T.; Abe, K. Characterization of the beta-D-glucopyranoside binding site of the human bitter taste receptor hTAS2R16. *J Biol Chem* **2010**, *285*, 28373–28378.

(49) Daura, X.; Mark, A. E.; Van Gunsteren, W. F. Parametrization of aliphatic CHn united atoms of GROMOS96 force field. *J Comput Chem* **1998**, *19*, 535–547.

(50) De Vries, S. J.; Van Dijk, M.; Bonvin, A. M. The HADDOCK web server for data-driven biomolecular docking. *Nature protocols* **2010**, *5*, 883.

(51) Zhukov, A.; Andrews, S. P.; Errey, J. C.; Robertson, N.; Tehan, B.; Mason, J. S.; Marshall, F. H.; Weir, M.; Congreve, M. Biophysical mapping of the adenosine A2A receptor. *J Med Chem* **2011**, *54*, 4312–4323.

(52) Dohlman, H. G.; Caron, M. G.; DeBlasi, A.; Frielle, T.; Lefkowitz, R. J. Role of extracellular disulfide-bonded cysteines in the ligand binding function of the. beta. 2-adrenergic receptor. *Biochemistry* **1990**, *29*, 2335–2342.

(53) Green, S. A.; Cole, G.; Jacinto, M.; Innis, M.; Liggett, S. A polymorphism of the human beta 2-adrenergic receptor within the fourth transmembrane domain alters ligand binding and functional properties of the receptor. *J Biol Chem* **1993**, *268*, 23116–23121.

(54) Liapakis, G.; Ballesteros, J. A.; Papachristou, S.; Chan, W. C.; Chen, X.; Javitch, J. A. The Forgotten Serine: A critical role for Ser-203$^{5.42}$ in ligand binding to and activation of the β2-adrenergic receptor. *J Biol Chem* **2000**, *275*, 37779–37788.

(55) Ferruz, N.; Doerr, S.; Vanase-Frawley, M. A.; Zou, Y.; Chen, X.; Marr, E. S.; Nelson, R. T.; Kormos, B. L.; Wager, T. T.; Hou, X.; Villalobos, A.; Sciabola, S.; De Fabritiis, G. Dopamine D3 receptor antagonist reveals a cryptic pocket in aminergic GPCRs. *Scientific reports* **2018**, *8*, 1–10.

(56) Van Zundert, G.; Rodrigues, J.; Trellet, M.; Schmitz, C.; Kastritis, P.; Karaca, E.; Melquiond, A.; van Dijk, M.; De Vries, S.; Bonvin, A. The HADDOCK2. 2 web server: user-friendly integrative modeling of biomolecular complexes. *J Mol Biol* **2016**, *428*, 720–725.

(57) Schrödinger Release 2017-3: Induced Fit Docking protocol. Glide, Schrödinger, LLC, New York, NY, 2017; Prime, Schrödinger, LLC, New York, NY, 2017.

(58) Söding, J. Protein homology detection by HMM–HMM comparison. *Bioinformatics* **2005**, *21*, 951–970.

(59) Sandal, M.; Duy, T. P.; Cona, M.; Zung, H.; Carloni, P.; Musiani, F.; Giorgetti, A. GOMoDo: a GPCRs online modeling and docking webserver. *PLOS ONE* **2013**, *8*, e74092.

(60) Waterhouse, A.; Bertoni, M.; Bienert, S.; Studer, G.; Tauriello, G.; Gumienny, R.; Heer, F. T.; de Beer, T. A. P.; Rempfer, C.; Bordoli, L.; Lepore, R.; Schwede, T. SWISS-MODEL: homology modelling of protein structures and complexes. *Nucleic Acids Res* **2018**, *46*, W296–W303.

(61) Webb, B.; Sali, A. Comparative protein structure modeling using MODELLER. *Curr Protoc Bioinformatics* **2016**, *54*, 5–6.

(62) Šali, A.; Blundell, T. L. Comparative protein modelling by satisfaction of spatial restraints. *J Mol Biol* **1993**, *234*, 779–815.

(63) Shen, M.-y.; Sali, A. Statistical potential for assessment and prediction of protein structures. *Protein science* **2006**, *15*, 2507–2524.

(64) Melo, F.; Sánchez, R.; Sali, A. Statistical potentials for fold assessment. *Protein science* **2002**, *11*, 430–448.

(65) John, B.; Sali, A. Comparative protein structure modeling by iterative alignment, model building and model assessment. *Nucleic Acids Res* **2003**, *31*, 3982–3992.

(66) Williams, C. J.; Headd, J. J.; Moriarty, N. W.; Prisant, M. G.; Videau, L. L.; Deis, L. N.; Verma, V.; Keedy, D. A.; Hintze, B. J.; Chen, V. B.; Jain, S.; Lewis, S. M.; Arendall III, W. B.; Snoeyink, J.; Adams, P. D.; Lovell, S. C.; Richardson, J. S.; Richardson, D. C. MolProbity: More and better reference data for improved all-atom structure validation. *Protein Science* **2018**, *27*, 293–315.

(67) Schüttelkopf, A. W.; Van Aalten, D. M. PRODRG: a tool for high-throughput crystallography of protein–ligand complexes. *Acta Crystallogr. D* **2004**, *60*, 1355–1363.

(68) Le Guilloux, V.; Schmidtke, P.; Tuffery, P. Fpocket: an open source platform for ligand pocket detection. *BMC bioinformatics* **2009**, *10*, 168.

(69) Kurkcuoglu, Z.; Koukos, P. I.; Citro, N.; Trellet, M. E.; Rodrigues, J.; Moreira, I. S.; Roel-Touris, J.; Melquiond, A. S.; Geng, C.; Schaarschmidt, J.; Xue, L. C.; Vangone, A.; Bonvin, A. M. J. J. Performance of HADDOCK and a simple contact-based protein–ligand binding affinity predictor in the D3R Grand Challenge 2. *J Comput Aided Mol Des* **2018**, *32*, 175–185.

(70) Koukos, P. I.; Xue, L. C.; Bonvin, A. M. Protein–ligand pose and affinity prediction: Lessons from D3R Grand Challenge 3. *J Comput Aided Mol Des* **2019**, *33*, 83–91.

(71) Vangone, A.; Schaarschmidt, J.; Koukos, P.; Geng, C.; Citro, N.; Trellet, M. E.; Xue, L. C.; Bonvin, A. M. Large-scale prediction of binding affinity in protein–small ligand complexes: the PRODIGY-LIG web server. *Bioinformatics* **2019**, *35*, 1585–1587.

(72) Berendsen, H. J. C.; van der Spoel, D.; van Drunen, R. GROMACS: a message-passing parallel molecular dynamics implementation. *Comput Phys Commun* **1995**, *91*, 43–56.

(73) Hess, B.; Kutzner, C.; Van Der Spoel, D.; Lindahl, E. GROMACS 4: algorithms for highly efficient, load-balanced, and scalable molecular simulation. *J Chem Theory Comput* **2008**, *4*, 435–447.

(74) Berendsen, H. J. C.; Grigera, J. R.; Straatsma, T. P. The missing term in effective pair potentials. *J Phys Chem* **1987**, *91*, 6269–6271.

(75) Hansen, H. S.; Hünenberger, P. H. A reoptimized GROMOS force field for hexopyranose-based carbohydrates accounting for the relative free energies of ring

conformers, anomers, epimers, hydroxymethyl rotamers, and glycosidic linkage conformers. *J Comput Chem* **2011**, *32*, 998–1032.

(76) Bayly, C. I.; Cieplak, P.; Cornell, W.; Kollman, P. A. A well-behaved electrostatic potential based method using charge restraints for deriving atomic charges: the RESP model. *J Phys Chem* **1993**, *97*, 10269–10280.

(77) Frisch, M. J.; Trucks, G. W.; Schlegel, H. B.; Scuseria, G. E.; Robb, M. A.; Cheeseman, J. R.; Scalmani, G.; Barone, V.; Mennucci, B.; Petersson, G. A.; Nakatsuji, H.; Caricato, M.; Li, X.; Hratchian, H. P.; Izmaylov, A. F.; Bloino, J.; Zheng, G.; Sonnenberg, J. L.; Hada, M.; Ehara, M.; Toyota, K.; Fukuda, R.; Hasegawa, J.; Ishida, M.; Nakajima, T.; Honda, Y.; Kitao, O.; Nakai, H.; Vreven, T.; Montgomery, J. A., Jr.; Peralta, J. E.; Ogliaro, F.; Bearpark, M.; Heyd, J. J.; Brothers, E.; Kudin, K. N.; Staroverov, V. N.; Kobayashi, R.; Normand, J.; Raghavachari, K.; Rendell, A.; Burant, J. C.; Iyengar, S. S.; Tomasi, J.; Cossi, M.; Rega, N.; Millam, J. M.; Klene, M.; Knox, J. E.; Cross, J. B.; Bakken, V.; Adamo, C.; Jaramillo, J.; Gomperts, R.; Stratmann, R. E.; Yazyev, O.; Austin, A. J.; Cammi, R.; Pomelli, C.; Ochterski, J. W.; Martin, R. L.; Morokuma, K.; Zakrzewski, V. G.; Voth, G. A.; Salvador, P.; Dannenberg, J. J.; Dapprich, S.; Daniels, A. D.; Farkas, Ö.; Foresman, J. B.; Ortiz, J. V.; Cioslowski, J.; Fox, D. J. Gaussian 09 Revision E.01. Gaussian Inc. Wallingford CT 2009.

(78) Wang, J.; Wang, W.; Kollman, P. A.; Case, D. A. Antechamber: an accessory software package for molecular mechanical calculations. *J Am Chem Soc* **2001**, *222*, U403.

(79) Lemkul, J. A.; Allen, W. J.; Bevan, D. R. Practical considerations for building GROMOS-compatible small-molecule topologies. *J Chem Inf Model* **2010**, *50*, 2221–2235.

(80) Jorgensen, W. L.; Chandrasekhar, J.; Madura, J. D.; Impey, R. W.; Klein, M. L.

Comparison of simple potential functions for simulating liquid water. *J Chem Phys* **1983**, *79*, 926–935.

(81) Jakalian, A.; Jack, D. B.; Bayly, C. I. Fast, efficient generation of high-quality atomic charges. AM1-BCC model: II. Parameterization and validation. *J Comput Chem* **2002**, *23*, 1623–1641.

(82) Lomize, M. A.; Pogozheva, I. D.; Joo, H.; Mosberg, H. I.; Lomize, A. L. OPM database and PPM web server: resources for positioning of proteins in membranes. *Nucleic Acids Res* **2012**, *40*, D370–D376.

(83) Schrödinger Release 2017-3: Maestro. Schrödinger, LLC, New York, NY, 2017.

(84) Olsson, M. H.; Sondergaard, C. R.; Rostkowski, M.; Jensen, J. H. PROPKA3: consistent treatment of internal and surface residues in empirical pKa predictions. *J Chem Theory Comput* **2011**, *7*, 525–537.

(85) Harder, E.; Damm, W.; Maple, J.; Wu, C.; Reboul, M.; Xiang, J. Y.; Wang, L.; Lupyan, D.; Dahlgren, M. K.; Knight, J. L.; Kaus, J. W.; Cerutti, D. S.; Krilov, G.; Jorgensen, W. L.; Abel, R.; Friesner, R. A. OPLS3: a force field providing broad coverage of drug-like small molecules and proteins. *J Chem Theory Comput* **2016**, *12*, 281–296.

(86) Schrödinger Release 2017-3: LigPrep. Schrödinger, LLC, New York, NY, 2017.

(87) Schrödinger Release 2017-3: Epik. Schrödinger, LLC, New York, NY, 2017.

(88) Chien, E. Y.; Liu, W.; Zhao, Q.; Katritch, V.; Han, G. W.; Hanson, M. A.; Shi, L.; Newman, A. H.; Javitch, J. A.; Cherezov, V.; Stevens, R. C. Structure of the human dopamine D3 receptor in complex with a D2/D3 selective antagonist. *Science* **2010**, *330*, 1091–1095.

(89) Schrödinger Release 2017-3: Glide. Schrödinger, LLC, New York, NY, 2017.

(90) Schrödinger Release 2017-3: Prime. Schrödinger, LLC, New York, NY, 2017.

(91) Humphrey, W.; Dalke, A.; Schulten, K. VMD: visual molecular dynamics. *J Mol Graph* **1996**, *14*, 33–38.

(92) Daura, X.; Gademann, K.; Jaun, B.; Seebach, D.; Van Gunsteren, W. F.; Mark, A. E. Peptide folding: when simulation meets experiment. *Angew Chem Int Ed* **1999**, *38*, 236–240.

(93) González-Alemán, R.; Hernández-Castillolo, D.; Caballero, J.; Montero-Cabrera, L. A. Quality threshold clustering of molecular dynamics: a word of caution. *J Chem Inf Model* **2019**, *60*, 467–472.

(94) Ballesteros, J. A.; Weinstein, H. *Methods in neurosciences*; Elsevier, 1995; Vol. 25; pp 366–428.

(95) The values of the statistical parameters for Amber-based MM/CG are always larger than or equal to the GROMOS-based MM/CG and docking ones, independently from the definition used.

(96) Thermostabilised adenosine A2A receptor in complex with caffeine - Experiment. `https://www.rcsb.org/experimental/3RFM`, [Online; accessed May 29th 2020].

(97) Fredriksson, K.; Lottmann, P.; Hinz, S.; Onila, I.; Shymanets, A.; Harteneck, C.; Müller, C. E.; Griesinger, C.; Exner, T. E. Nanodiscs for INPHARMA NMR characterization of GPCRs: ligand binding to the human A2A adenosine receptor. *Angewandte Chemie* **2017**, *129*, 5844–5848.

(98) Sabbadin, D.; Ciancetta, A.; Moro, S. Bridging molecular docking to membrane molecular dynamics to investigate GPCR–ligand recognition: the human A2A adenosine receptor as a key study. *J Chem Inf Model* **2014**, *54*, 169–183.

(99) Igonet, S.; Raingeval, C.; Cecon, E.; Pučić-Baković, M.; Lauc, G.; Cala, O.; Baranowski, M.; Perez, J.; Jockers, R.; Krimm, I.; Jawhari, A. Enabling STD-NMR fragment screening using stabilized native GPCR: A case study of adenosine receptor. *Scientific reports* **2018**, *8*, 1–14.

(100) GPCRmd all-atom MD simulations. `http://submission.gpcrmd.org/dynadb/dynamics/id/38/`, [Online; accessed April 23rd 2020].

(101) Suku, E.; Giorgetti, A. Common evolutionary binding mode of rhodopsin-like GPCRS: Insights from structural bioinformatics. *AIMS Press, AIMS. Biophysics* **2017**, *4*, 543–556.

(102) Suryanarayana, S.; Kobilka, B. K. Amino acid substitutions at position 312 in the seventh hydrophobic segment of the beta 2-adrenergic receptor modify ligand-binding specificity. *Mol Pharmacol* **1993**, *44*, 111–114.

(103) Wieland, K.; Zuurmond, H. M.; Krasel, C.; Ijzerman, A. P.; Lohse, M. J. Involvement of Asn-293 in stereospecific agonist recognition and in activation of the beta 2-adrenergic receptor. *Proc Natl Acad Sci U S A* **1996**, *93*, 9276–9281.

(104) Lakkaraju, S. K.; Lemkul, J. A.; Huang, J.; MacKerell Jr, A. D. DIRECT-ID: An automated method to identify and quantify conformational variations—application to β2-adrenergic GPCR. *J Comput Chem* **2016**, *37*, 416–425.

(105) Chan, H. S.; Filipek, S.; Yuan, S. The Principles of Ligand Specificity on beta-2-adrenergic receptor. *Scientific reports* **2016**, *6*, 34736.

(106) Huber, T.; Menon, S.; Sakmar, T. P. Structural basis for ligand binding and specificity in adrenergic receptors: implications for GPCR-targeted drug discovery. *Biochemistry* **2008**, *47*, 11013–11023.

(107) Feng, Z.; Hou, T.; Li, Y. Selectivity and activation of dopamine D3R from molecular dynamics. *J Mol Model* **2012**, *18*, 5051–5063.

(108) Bueschbell, B.; Barreto, C. A.; Preto, A. J.; Schiedel, A. C.; Moreira, I. S. A Complete Assessment of Dopamine Receptor-Ligand Interactions through Computational Methods. *Molecules* **2019**, *24*, 1196.

(109) Strader, C. D.; Candelore, M.; Hill, W.; Sigal, I.; Dixon, R. Identification of two serine residues involved in agonist activation of the beta-adrenergic receptor. *J Biol Chem* **1989**, *264*, 13572–13578.

(110) Loo, J. S.; Emtage, A. L.; Ng, K. W.; Yong, A. S.; Doughty, S. W. Assessing GPCR homology models constructed from templates of various transmembrane sequence identities: Binding mode prediction and docking enrichment. *J Mol Graph Model* **2018**, *80*, 38–47.

(111) Jaiteh, M.; Rodríguez-Espigares, I.; Selent, J.; Carlsson, J. Performance of virtual screening against GPCR homology models: Impact of template selection and treatment of binding site plasticity. *PLOS Comput Biol* **2020**, *16*, e1007680.

(112) Ciancetta, A.; Cuzzolin, A.; Moro, S. Alternative quality assessment strategy to compare performances of GPCR-ligand docking protocols: the human adenosine A2A receptor as a case study. *J Chem Inf Model* **2014**, *54*, 2243–2254.

(113) Rodríguez, D.; Ranganathan, A.; Carlsson, J. Discovery of GPCR ligands by molecular docking screening: novel opportunities provided by crystal structures. *Curr Top Med Chem* **2015**, *15*, 2484–2503.

(114) Lenselink, E. B.; Beuming, T.; Sherman, W.; van Vlijmen, H. W.; IJzerman, A. P. Selecting an optimal number of binding site waters to improve virtual screening enrichments against the adenosine A2A receptor. *J Chem Inf Model* **2014**, *54*, 1737–1746.

(115) Orgován, Z.; Ferenczy, G. G.; Keserű, G. M. The role of water and protein flexibility in the structure-based virtual screening of allosteric GPCR modulators: an mGlu 5 receptor case study. *J Comput Aided Mol Des* **2019**, *33*, 787–797.

(116) Rudling, A.; Orro, A.; Carlsson, J. Prediction of Ordered Water Molecules in Protein Binding Sites from Molecular Dynamics Simulations: The Impact of Ligand Binding on Hydration Networks. *J Chem Inf Model* **2018**, *58*, 350–361.

(117) Venkatakrishnan, A.; Ma, A. K.; Fonseca, R.; Latorraca, N. R.; Kelly, B.; Betz, R. M.; Asawa, C.; Kobilka, B. K.; Dror, R. O. Diverse GPCRs exhibit conserved water networks for stabilization and activation. *Proc Natl Acad Sci U S A* **2019**, *116*, 3288–3293.

(118) Tarenzi, T.; Calandrini, V.; Potestio, R.; Carloni, P. Open-Boundary Molecular Mechanics/Coarse-Grained Framework for Simulations of Low-Resolution G-Protein-Coupled Receptor–Ligand Complexes. *J Chem Theory Comput* **2019**, *15*, 2101–2109.

(119) Schneider, J.; Ribeiro, R.; Alfonso-Prieto, M.; Carloni, P.; Giorgetti, A. Hybrid MM/CG Webserver: Automatic set up of molecular mechanics/coarse-grained simulations for human G protein-coupled receptor/ligand complexes. *submitted* **2020**,

Graphical TOC Entry